INTERNATIONAL JOURNAL FOR NUMERICAL METHODS IN ENGINEERING
Int. J. Numer. Meth. Engng 2002; **53**:2501–2528 (DOI: 10.1002/nme.404)

Remeshing for metal forming simulations—Part II: Three-dimensional hexahedral mesh generation

Dae-Young Kwak[1,†] and Yong-Taek Im[2,*,‡]

[1] *Passenger Car Chassis and Powertrain Engineering Team 3, Research and Development Division for Hyundai Motor Company and Kia Motors Corporation, 781-1, Soha-dong, Kwangmyung-Shi, Kyunggi-Do, 423-701, South Korea*
[2] *Computer Aided Materials Processing Laboratory, Department of Mechanical Engineering, Korea Advanced Institute of Science and Technology, ME3227, 373-1 Kusong-dong, Yusong-gu, Taejon 305-701, South Korea*

SUMMARY

In the present study, a hexahedral mesh generator was developed for remeshing in three-dimensional metal forming simulations. It is based on the master grid approach and octree-based refinement scheme to generate uniformly sized or locally refined hexahedral mesh system. In particular, for refined hexahedral mesh generation, the modified Laplacian mesh smoothing scheme mentioned in the two-dimensional study (Part I) was used to improve the mesh quality while also minimizing the loss of element size conditions. In order to investigate the applicability and effectiveness of the developed hexahedral mesh generator, several three-dimensional metal forming simulations were carried out using uniformly sized hexahedral mesh systems. Also, a comparative study of indentation analyses was conducted to check the computational efficiency of locally refined hexahedral mesh systems. In particular, for specification of refinement conditions, distributions of effective strain-rate gradient and *posteriori* error values based on a Z^2 error estimator were used. From this study, it is construed that the developed hexahedral mesh generator can be effectively used for three-dimensional metal forming simulations. Copyright © 2002 John Wiley & Sons, Ltd.

KEY WORDS: metal forming simulation; three-dimensional remeshing; hexahedral mesh generation; hexahedral mesh refinement; modified Laplacian mesh smoothing

1. INTRODUCTION

As the finite element method has become one of the most popular tools to solve various engineering problems, mesh generation for complicated geometries has become an important

*Correspondence to: Yong-Taek Im, Department of Mechanical Engineering, ME3227, Korea Advanced Institute of Science and Technology, 373-1 Kusong-dong, Yusong-gu, Taejon 305-701, South Korea
†E-mail: kdy_kia@hanmail.net
‡E-mail: ytim@mail.kaist.ac.kr

Contract/grant sponsor: BK21 Project

Received 31 October 2000
Revised 28 May 2001

issue [1–5]. In particular, since successive remeshing processes are required in metal forming simulations, mesh generation becomes a necessary prerequisite for development of metal forming simulation system.

Mesh generation algorithms for complicated three-dimensional solids generally produce tetrahedral or hexahedral elements or a combination of these two types. Usually, a mesh is constrained in terms of elements requiring to share common facets, that is, the conformity condition must be satisfied. In this regard, tetrahedral and mixed element meshing algorithms are less constrained compared to hexahedral algorithms; hence, many robust and stable automatic mesh generation algorithms, such as Delaunay triangulation [6–10], octree decomposition [11–15], and advancing front technique [16–18] have been successfully developed.

Up to now, a great number of schemes have been developed for hexahedral mesh generation, but unfortunately, none of them are perfect in terms of robustness or automation. The existing schemes can be classified into following three categories. The first category is based on the mapping/sweeping scheme for generation of all-structured hexahedral mesh systems [19–24]. The second category is based on the plastering [25–27] and whisker-weaving [28–31] algorithms. In particular, the plastering scheme is a type of three-dimensional advancing front technique applied to hexahedral elements. And the other well-known category is the grid-based approach, which involves initial grid generation, removal of exterior elements, and boundary mesh fitting [32, 33]. Although grid-based approaches produce well-shaped structured elements in the interior of solids, they generally produce poorly shaped elements on the boundary. In spite of such undesirable features, many studies have been carried out in this category because the approach is somewhat simple to implement and more suitable for most mesh generation problems. As a result, considerable progress in this approach has been achieved.

Apart from these, it is well-known that adaptive finite element analysis with error estimation is a very important research issue in the field of many engineering problems. In particular, in the finite element analysis of metal forming processes, as local stress concentrations and severe deformations due to contact between dies and the workpiece occur frequently, an adaptive analysis can be significantly beneficial in achieving more accurate and efficient simulations.

Adaptive analysis has usually taken the form of one of the following [34]. The most common method is *h-adaptation* which reduces the element size in a specified region to improve the solution accuracy. Another method is *p-adaptation* which increases the polynomial order of the shape function without changing the initial mesh configuration. Some authors introduced *r-adaptation* in which an initial mesh is modified by changing the position of nodes to achieve improvement in accuracy.

Mesh refinement is a procedure in which an initial solution is computed for a coarse mesh system which is then refined in specific regions where the solution errors are too large. In this sense, mesh refinement can simply be considered to be equivalent with *h-adaptation*. Many studies have been carried out for such mesh refinement procedure, but most focused on two-dimensional triangular and quadrilateral or three-dimensional tetrahedral elements [35–41]. This is because for these elements, an adaptive mesh generation process is less complicated and constrained compared to the case of hexahedral elements due to geometrical simplicity.

The adaptive hexahedral mesh generation algorithms that have been developed to this day possess a certain amount of limitations. Yang *et al.* [42] proposed the modular mesh generation

scheme in which hexahedral mesh systems were generated by the use of combinations of various module libraries. They applied the scheme for analyses of bevel gear forging and flat die extrusion, and it was shown that this scheme is quite effective for metal forming analyses. However, this scheme has the limitation in the sense of automation due to the complexity incurred in the course of combining the various modules. In another study, Schneider *et al.* [32] proposed the octree-based hexahedral mesh refinement scheme. This approach is similar to the modular scheme in that transition templates are used to meet the geometric conformity condition, but it has the merit that automation of refinement can be easily achieved due to the characteristics of the octree-based level structure in recursive decomposition.

In the present study, a hexahedral mesh generator based on the master grid approach and octree-based refinement scheme was developed as part of a three-dimensional metal forming analysis system, CAMP*form*-3*D* [43]. The finite element solver for CAMP*form*-3*D* was based on the thermo-rigid–viscoplastic approach and constant shear friction model was implemented at the dies and workpiece interface [44, 45]. The developed hexahedral mesh generator was designed to be applied for both uniformly sized and locally refined hexahedral mesh systems. The development of the hexahedral mesh generator based on the master grid approach and octree-based hexahedral mesh refinement will be explained in Sections 2 and 3. And the results of several metal forming simulation examples using uniformly sized or locally refined mesh systems will be discussed in Section 4.

2. PROCEDURE OF MASTER GRID APPROACH

As mentioned, one of the hexahedral mesh generators developed in this study is based on the master grid approach proposed by Lee *et al.* [33]. The main idea and algorithm of the master grid approach are similar to those of other conventional grid-based approaches, but they proposed the following two concepts desirable for metal forming simulations.

First, as its name suggests, the initial core mesh system is similar in shape to the original solid geometry, so that robustness of mesh generation and boundary element quality can be improved compared to conventional cases that use cubical cores. Also, this concept can be extended to locally refined mesh system. That is, a refined core mesh can be used to efficiently generate locally refined hexahedral mesh system.

Second, the master grid approach is able to generate well-shaped elements near the geometric boundary by using the concept of surface element layer (SEL). This SEL generation process has subdued the irregularity of poorly shaped boundary elements. As a result, hexahedral mesh system that is suitable for the finite element analysis of metal forming processes can be generated.

Figure 1 shows the overall procedure of the hexahedral mesh generation process. As shown in this figure, hexahedral mesh generation is carried out through the following six steps.

2.1. Boundary surface construction

When the input of the degenerated hexahedral mesh system is given in a specified format, a boundary surface enclosing the mesh system is constructed by a triangular surface mesh system. Figure 2 shows the procedure of the boundary surface construction process.

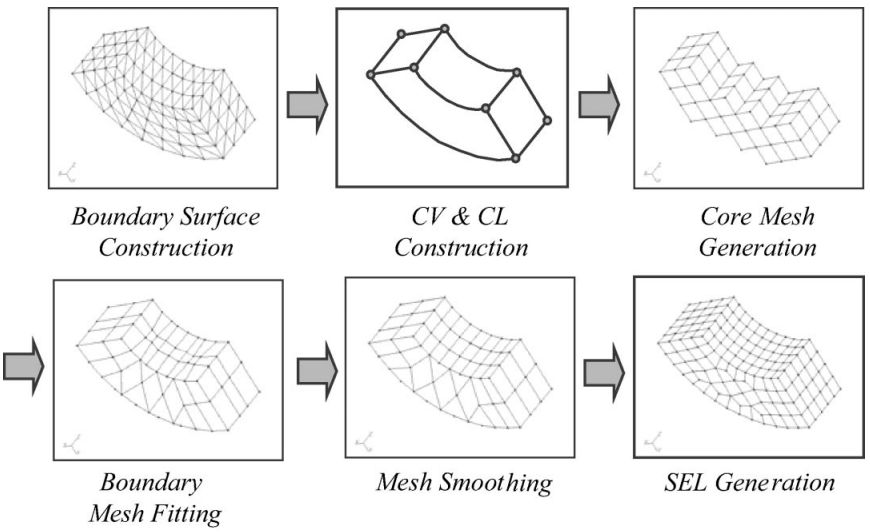

Figure 1. Overall procedure of the hexahedral mesh generation process.

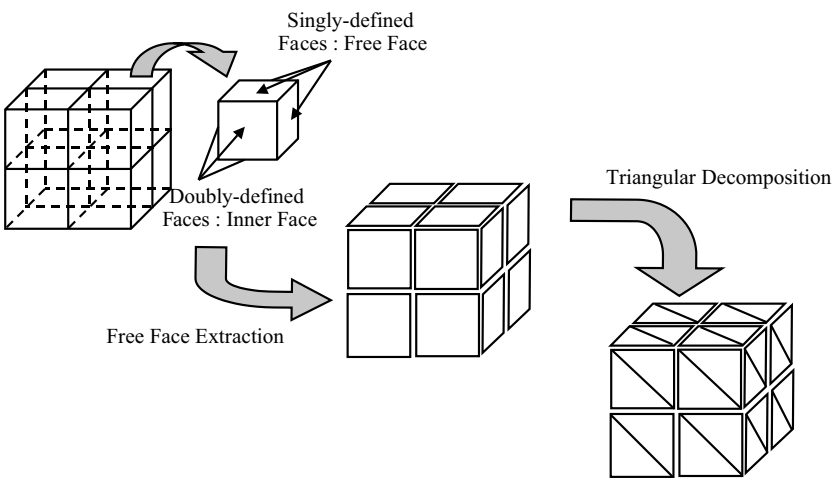

Figure 2. Schematic diagram of boundary surface construction.

As shown in Figure 2, this process is conducted through free face extraction and triangular decomposition.

Hexahedral elements have six quadrilateral faces. Each face can be classified into singly or doubly defined by the number of attached elements. Then, singly defined and doubly defined faces can be recognized as free and internal faces, respectively. In this way, free faces can be easily extracted and collected to determine the boundary of the solid object. Finally, triangular

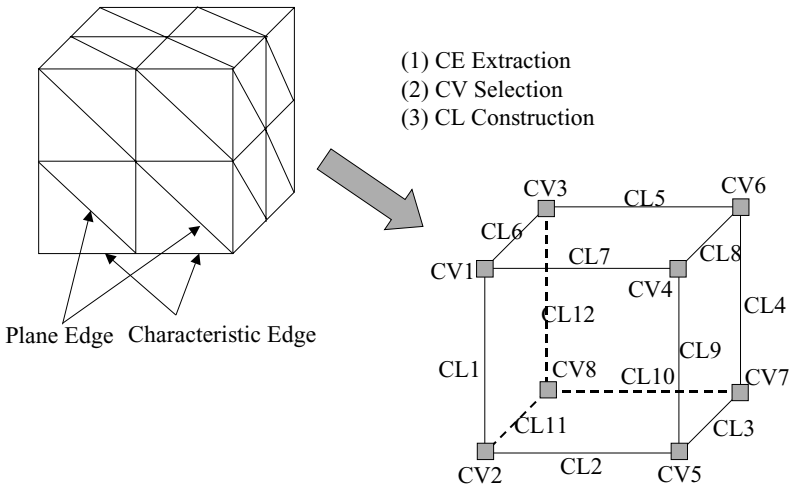

Figure 3. Schematic diagram of CV and CL construction process.

decomposition is carried out by dividing the quadrilateral free faces in the shorter diagonal direction.

2.2. *Characteristic vertex* (*CV*) *and characteristic line* (*CL*) *construction*

Usually, a three-dimensional workpiece model used in metal forming contains sharp corner points and edges. Apart from inherently existing sharp points or edges, many such singularities are induced from the treatment of symmetric characteristics during FEM analyses. More specifically, metal forming products usually contain planes of symmetry that can be made use of to decrease computational time during FEM analysis. That is, depending on geometrical symmetry only $\frac{1}{2}$, $\frac{1}{4}$, or $\frac{1}{8}$ models of the original workpiece model can be used with appropriate boundary conditions. Dividing the workpiece by the planes of symmetry results in the generation of sharp corner points and edges in such regions. For example, a sharp edge is formed at the intersection of two symmetric planes and a sharp corner point is created at the intersection point of three symmetric planes.

These sharp points and edges cause problems in the surface treatment, more precisely, a unique normal vector does not exist at these points and edges. Thus, for special treatment of such points and edges, existing sharp corner points and edges are extracted and classified as *characteristic vertex* (CV) and *characteristic edge* (CE), respectively.

Figure 3 describes the process of CV and CL construction. As shown, this process is carried out through the following three steps. (i) *CE extraction*: an edge where the angle between the normal vectors of adjacent triangular elements is larger than a critical value is defined as a characteristic edge (CE). (ii) *CV selection*: a point which is connected to three CEs is defined as a CV. (iii) *CL construction*: the sequence of CEs starting from an arbitrary CV and ending at another CV. The generation of CVs and CLs is made in an arbitrary order, so the numberings of CVs and CLs shown in Figure 3 have no particular meaning.

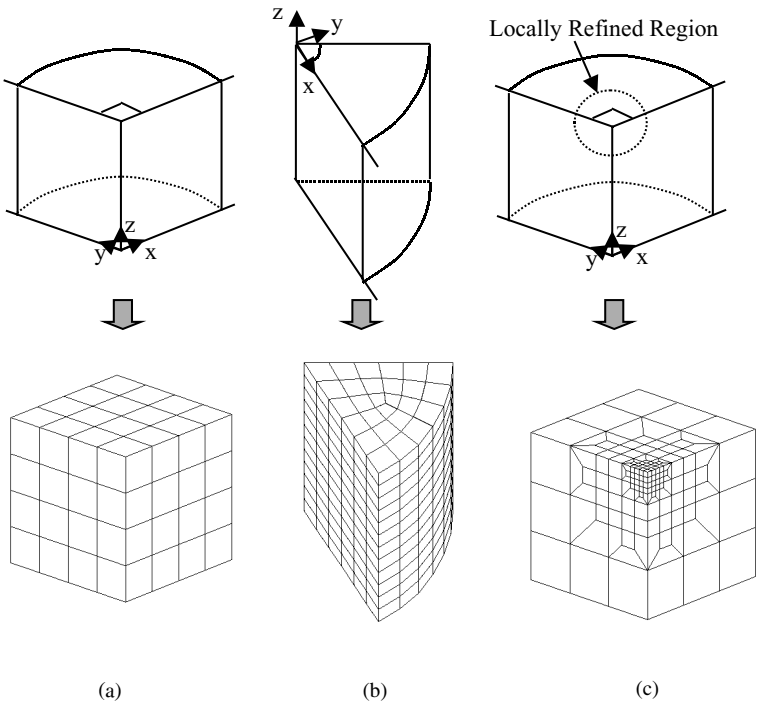

Figure 4. Typical examples of: (a) a structured grid system; (b) an unstructured grid system; and (c) a locally refined grid system used in the core mesh generation step.

2.3. *Core mesh generation*

As mentioned, most of the works using the grid-based approach used fully structured core mesh systems, in which a solid object is enclosed by equally sized hexahedral elements. Such a fully structured core mesh system is easy to construct and provides good meshes for many cases. However, in some metal forming analyses, the angle between symmetric planes of the workpiece may not be 90°, and thus such fully structured core mesh systems are not adequate. For example, in the case where symmetric planes of the workpiece do not coincide with the *yz*-plane, but only with *xz*-plane, core meshes are made in a wedge shape to better describe the workpiece geometry as shown in Figure 4(b). Therefore, in this investigation, fully structured and unstructured but less regular cores shown in Figure 4(a) and (b) were used as the initial core mesh system. In addition, for locally refined hexahedral mesh generation, a locally refined initial core as shown in Figure 4(c) was used in this study.

The construction of the initial core mesh system enclosing the solid object is followed by the removal process of exterior cells. This removal process is conducted by superimposing the initial core mesh system over the solid object and taking the grid points and core elements in the interior region as the nodes and elements, respectively. In order to determine whether a certain core element is in the interior region of a solid object, the status of the eight grid

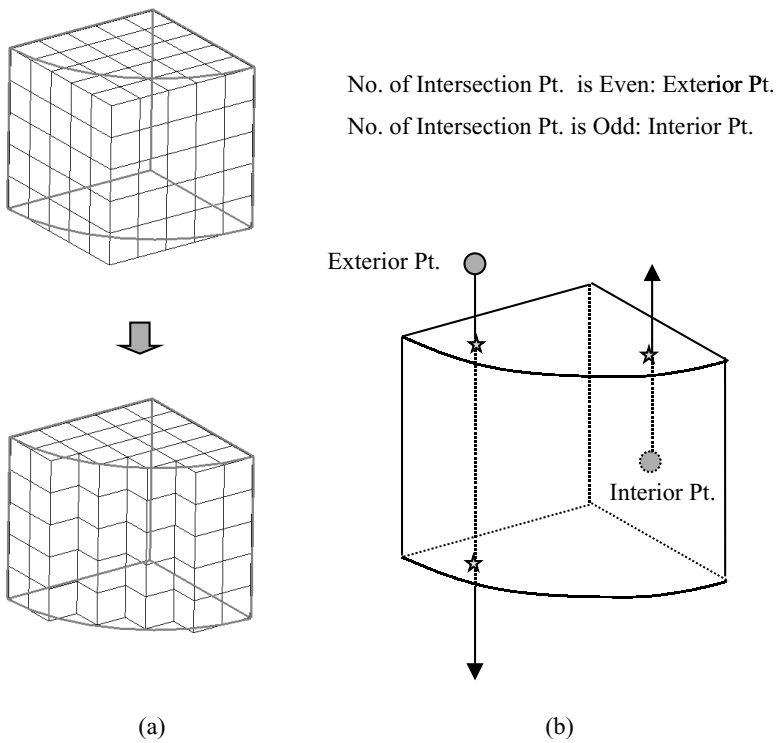

Figure 5. Schematic diagrams of: (a) core mesh generation; and (b) the even and odd parity rules.

points composing the cell is examined, and then the status of the cell is determined by the number of interior grid points. Figure 5(a) shows the concept of this process.

The status of grid points, that is, whether they are in the interior or exterior of the solid, is determined by the even and odd parity rule. The algorithm for this even and odd parity check is as follows:

Algorithm for even and odd parity check:

For $i = 1$, *all grid points of the core mesh system*
  For $j = 1$, *all triangle surface elements*
    Create an infinite line of any direction L_i *starting at the* ith *grid position*
    If L_i *intersects the* jth *triangle element and the* ith *grid is not on the* jth *triangle element, then* $count_i = count_i + 1$
  Next j
  If $count_i$ *is odd, then the* ith *grid point is in the interior*
  Otherwise, the ith *grid point is in the exterior*
Next i

Figure 5(b) shows examples of grid points determined as interior and exterior grid points using this rule.

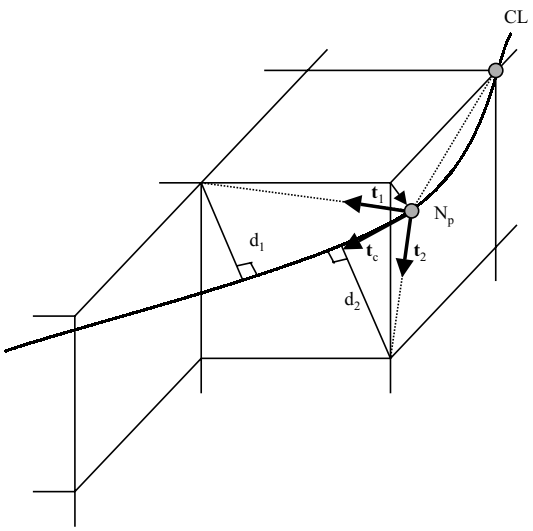

Figure 6. Schematic description of the recursive searching scheme.

2.4. *Boundary mesh fitting*

Since the generated core mesh system from the previous steps is composed of rugged shaped boundary elements that do not follow the shape of the old mesh geometry, every node on the boundary is enforced to move to the boundary surface. This process is conducted through three fitting steps, namely, (i) create *characteristic vertex nod*e (CVN) by moving the closest node to each CV to the position of the corresponding CV, (ii) adjust nodes near each CL by a proper tracing algorithm, and (iii) fit the remaining boundary nodes by a projection technique.

In particular, the tracing algorithm for stage (ii) selects the best qualified node among the nodes attached to a CVN as the next node and this next node is projected onto the CL. This searching process for the next node is recursively continued until another CVN is reached. Figure 6 describes this process of selecting the next candidate node after the node N_p has been projected onto the CL. The next best qualified node is selected as the node which minimizes the following function:

$$f = (1 - \mathbf{t}_c \cdot \mathbf{t}_i) + \frac{d_i}{\max(d_1, d_2, C_0)} \quad \text{for } i = 1, 2 \tag{1}$$

Here, d_i is the distance from a candidate node to the CL and $\mathbf{t}_i$ and $\mathbf{t}_c$ are the normalized vector in the edge direction and the normalized tangent vector of the CL, respectively. And C_0 is a positive constant set as the given element size during the core mesh generation process. The first term in Equation (1) indicates that the node with tangential direction $\mathbf{t}_i$ that is closest to the direction of $\mathbf{t}_c$ will be chosen as the next candidate node. And the second term, which is normalized using $\max(d_1, d_2, C_0)$, indicates that the node which is closest to the current node N_p will be chosen. Thus, Equation (1) physically means that the closer node directed in almost the same direction as the CL will be chosen as the next qualified node.

2.5. Mesh smoothing

Owing to compulsive movement of the boundary nodes, the generated hexahedral elements are poorly shaped near the boundary surface. Therefore, a smoothing technique that moves all such nodes to improve the global quality of the mesh system is carried out. More specifically, this process involves the three steps of (i) smoothing all nodes projected onto the CL, (ii) smoothing remaining boundary nodes and (iii) smoothing all interior nodes.

For smoothing nodes projected onto the CL, the positions of nodes are determined in the following manner. If k is the number of nodes on the CL, then the positions of the first node N_0 and the last node N_{k-1} are fixed while the other nodes in between are moved to new positions by the following equation:

$$\sum_{i=1}^{k-1}\left(\int_0^s \frac{\mathrm{d}s}{h_i(s)}\right)=m, \quad m=1,\ldots,k-2 \tag{2}$$

Here, s is a parametric value varying from 0 to 1 and $h_i(s)$ is the element size function defined on a segment between two nodes N_{i-1} and N_i. The element size function, $h_i(s)$, is defined as $h_i(s)=sh_2+(1-s)h_1$ where h_1 and h_2 are the element size values at nodes N_{i-1} and N_i, respectively. The $\mathrm{d}s/h_i(s)$ in the integral indicates the number of elements per unit length, and thus integrating from $s=0$ to 1 gives the total number of elements on the segment between nodes N_{i-1} and N_i. And by summing from $i=1$ to $k-1$, the left-hand side of Equation (2) indicates the total number of elements on the CL. Therefore, by finding the segment and the corresponding value of s that satisfies Equation (2) for $m=1$ will give the position of node N_1. This same procedure was applied for increasing values of m until $m=k-2$ to find all nodal positions (see Figure 7).

Secondly, for smoothing of the remaining boundary nodes, the modified Laplacian smoothing scheme proposed in the two-dimensional study (Part 1) is used. The conventional volume-weighted Laplacian smoothing scheme can be successfully used to improve the mesh quality, but it has the risk of not following the specified element size condition for locally refined mesh system. Thus, in order to complement such deficiency, the following repositioning equation was used in this study:

$$\begin{aligned} P_{\mathrm{new}} &= w\frac{\sum_{k=1}^{m}\mathbf{C}_k A_k}{\sum_{k=1}^{m}A_k}+(1-w)\frac{\sum_{k=1}^{n}\mathbf{X}_k W_k}{\sum_{k=1}^{m}W_k} \\ W_k &= 2/(S_k+S_0) \end{aligned} \tag{3}$$

Here, m and n are the number of adjacent free faces and adjacent nodes on the free faces, respectively. $\mathbf{C}_k$ and A_k are the centre position and area of each adjacent face, respectively. S_0 is the element size value of the node to be repositioned, and S_k and $\mathbf{X}_k$ are the element size and position of each adjacent node, respectively as shown in Figure 8. And w is a constant value ranging from 0 to 1. Since the node may not be on the boundary after the smoothing movement, the node should be projected onto the boundary surface.

After smoothing the boundary nodes from the previous steps, smoothing of interior nodes is carried out in a similar manner for the remaining boundary node smoothing as follows: Equation (3) was used again except that the terms of adjacent free faces were replaced with those of adjacent hexahedral elements. That is, m becomes the number of hexahedral

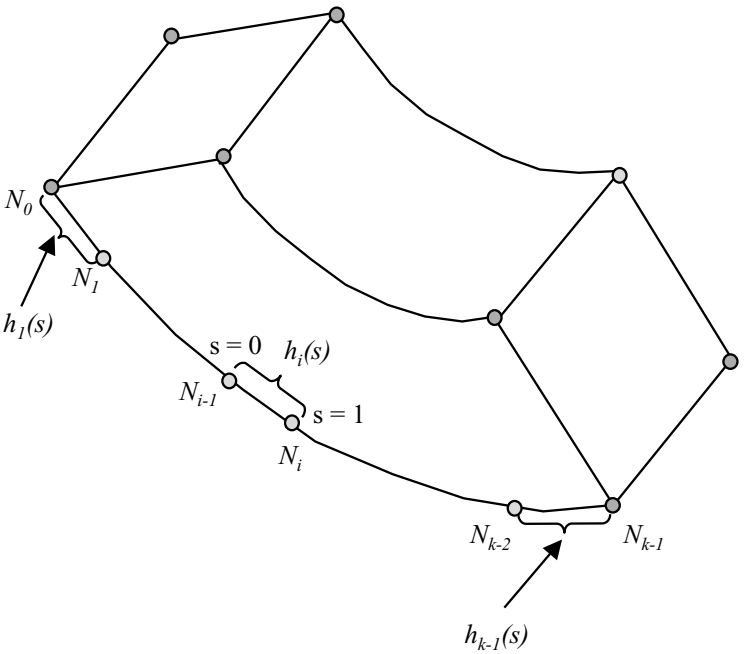

Figure 7. Schematic description of the smoothing of node positions on CL.

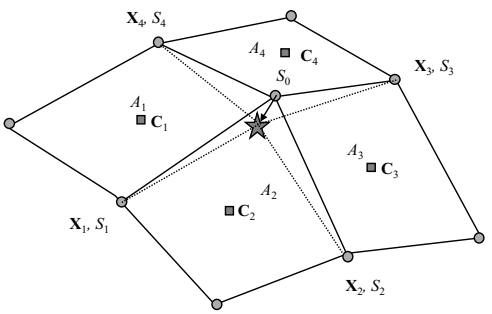

Figure 8. Schematic description of the determination of a new node location for remaining boundary node smoothing.

elements surrounding the node, n the number of adjacent nodes, and A_k the volume of each adjacent element.

2.6. *Surface element layer* (*SEL*) *generation*

As previously mentioned, one of the major defects of conventional grid-based mesh generation is that poorly shaped or severely distorted elements are often generated at the boundary due

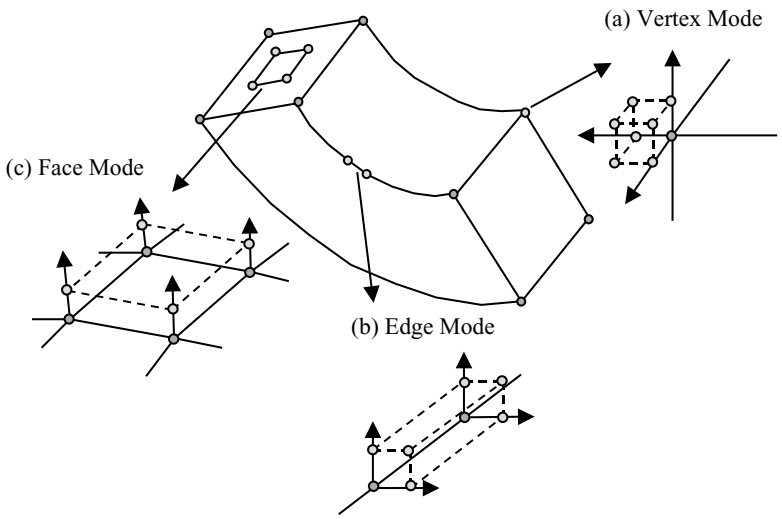

Figure 9. Schematic descriptions of three SEL modes and the generation method for each mode: (a) vertex; (b) edge; and (c) face modes.

to the compulsive boundary fitting process. Thus, in order to resolve this problem and make the approach more boundary sensitive, the concept of the surface element layer (SEL) with zero thickness was introduced.

In this study, the entire boundary mesh system is wrapped by surface elements with zero thickness, and then repositioning of all nodes is conducted by the smoothing process. This process has the effect of moving the original poorly shaped boundary elements into the interior region resulting in improvement of the quality of boundary elements.

The elements of SEL are generated by creating new nodes in the identical position of existing boundary nodes. However, depending on the type of boundary node the number of newly created nodes for the SEL should be different in order to meet the requirements of conformity. The three different modes of SEL generation depending on the type of boundary node, namely, (i) vertex, (ii) edge, and (iii) face modes, are illustrated in Figure 9. As can be seen, for vertex, edge, and face modes 7, 3, and 1 new SEL nodes need to be created, respectively. Although this figure displays the SEL with a finite thickness, this is only for display purpose. The newly created SEL elements will actually have zero thickness since all nodes will be at the same position of corresponding boundary nodes.

2.7. Mesh generation example

Figure 10 illustrates the procedure of uniformly sized hexahedral mesh generation for remeshing at an intermediate stage of spur gear forging simulation. In this case, remeshing was required due to degenerated elements in the region indicated by the dashed box shown in Figure 10(a).

After the old mesh system was given as the input geometry, triangular boundary mesh system and CV/CL were constructed as shown in Figures 10(b) and (c), respectively. The core mesh system was obtained by firstly constructing a cube-shaped hexahedral mesh system

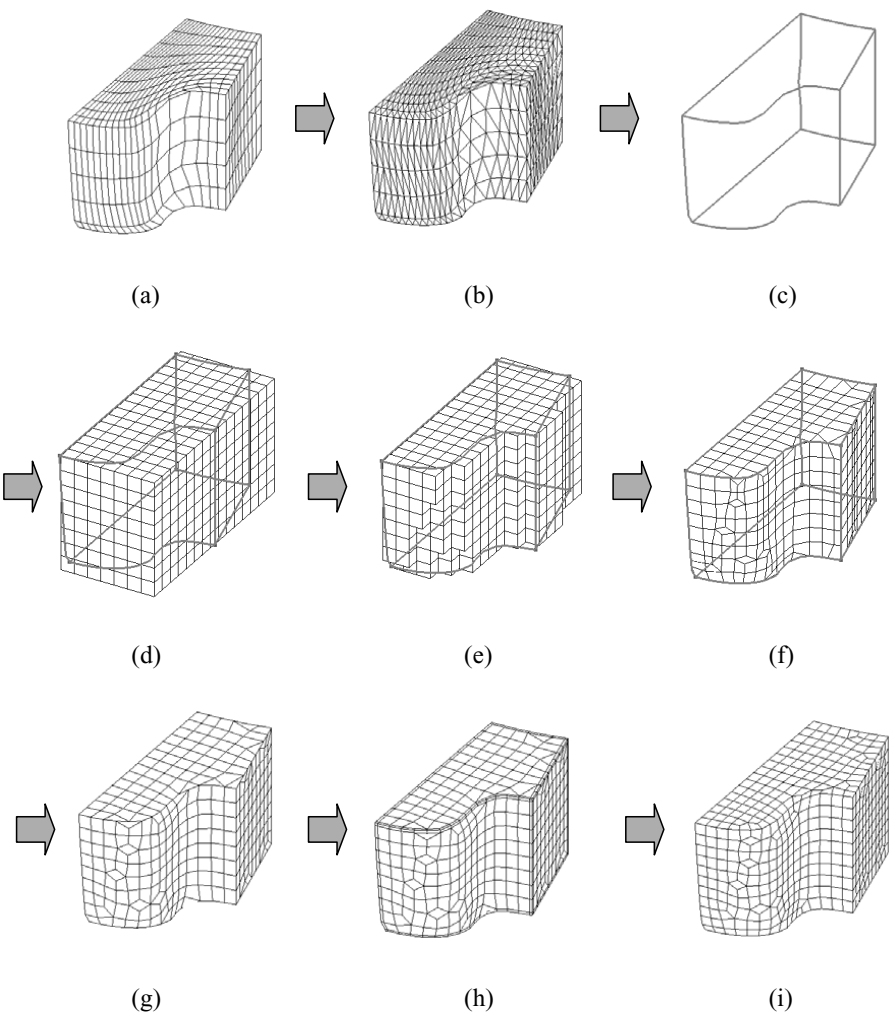

Figure 10. The procedure of uniformly sized hexahedral mesh generation for remeshing at an intermediate stage of spur gear forging simulation: (a) old mesh; (b) triangular boundary mesh; (c) CV/CL; (d) initial core mesh; (e) core mesh after removal of exterior elements; (f) boundary fitted mesh; (g) boundary fitted mesh after smoothing; (h) SEL generated mesh; and (i) final mesh.

enclosing the boundary surface and then removing the exterior elements as shown in Figures 10(d) and (e), respectively. Figures 10(f) and (g) show the boundary fitted mesh system before and after smoothing, respectively. It can be seen that the mesh system of Figure 10(g) has poorly shaped elements near the boundary surface. The final mesh system with well-shaped boundary elements was finally obtained by applying SEL generation as shown in Figure 10(h). The SEL generation process is shown step by step in Figure 11. Although this figure displays the SEL with a finite thickness, this is only for display purpose, as it actually has zero thickness.

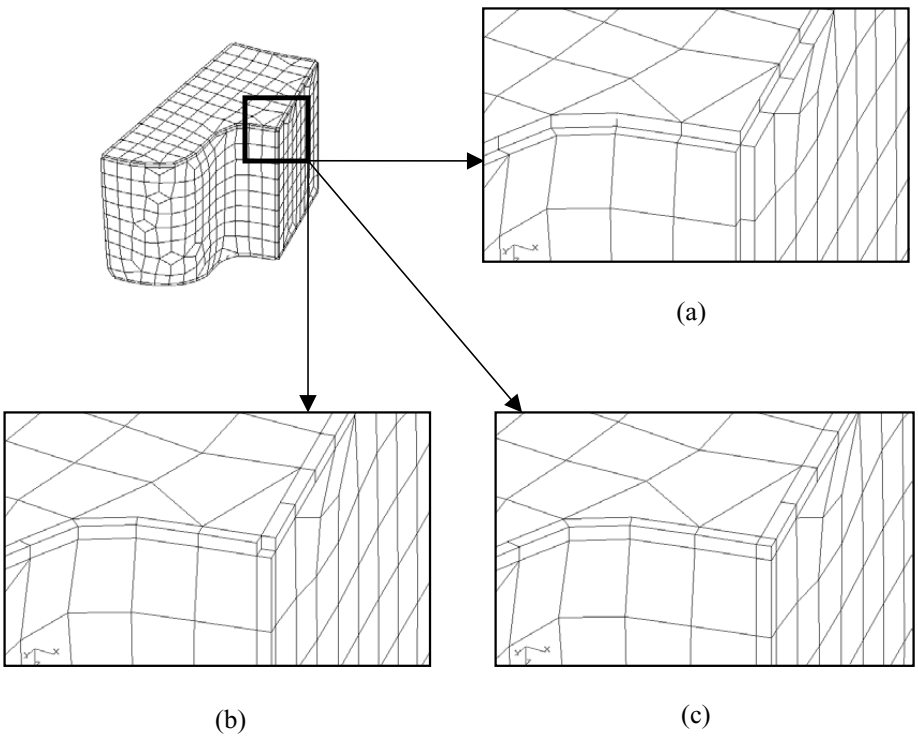

Figure 11. Illustration of the SEL generation process: (a) face mode; (b) edge mode; and (c) vertex mode.

3. HEXAHEDRAL MESH REFINEMENT

In general, an adaptive analysis means that the solution accuracy is improved while computational cost is minimized through adaptation of the finite element model according to the characteristics of the given engineering problem. In particular, in metal forming analyses, as local stress concentrations and severe deformations due to contact with dies frequently occur, an adaptive analysis can significantly improve the accuracy and efficiency of the analysis. Therefore, in the present investigation, for development of an adaptive hexahedral mesh generator, an octree-based hexahedral mesh refinement scheme was implemented into the developed hexahedral mesh generator.

The main idea of the octree-based refinement scheme is to construct an initial octree structure by recursive decomposition process in accordance to the prescribed element size conditions and then to convert each octant into a hexahedral element. During the conversion process, appropriate transition templates are inserted in order to satisfy the geometric conformity condition. Figure 12 shows the entire refinement procedure.

3.1. Initial octree construction

The refinement scheme used in this study is based on the study by Schneider *et al.* [32], but with a small modification. In their study, a bounding cube that contains the entire solid object

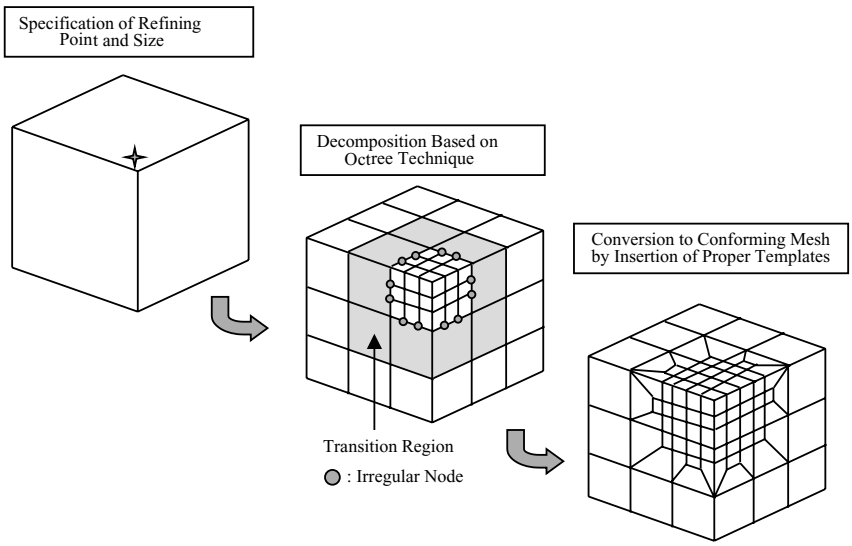

Figure 12. Schematic diagram of the octree-based mesh refinement procedure.

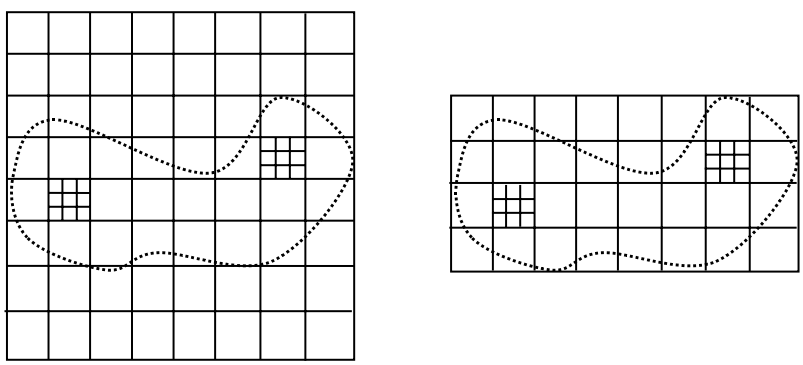

Figure 13. Schematic description of the: (a) conventional octree; and the (b) modified octree structure using a bounded grid system.

was chosen as the root octant, and recursive decomposition was carried out until the specified size conditions were satisfied. This can lead to the generation of a great number of unnecessary exterior elements if the aspect ratio of the bounding hexahedron enclosing the solid geometry is large. In order to resolve this problem, a uniformly sized grid system bounding the solid geometry is generated in a similar manner as that in the core mesh generation process prior to the recursive decomposition step in this investigation. Figure 13 describes the difference between these two schemes in two-dimensional sense.

For recursive decomposition at the local regions, element size conditions should be specified in an appropriate manner. For this purpose, the subdivision level of each octant is firstly defined as follows:

Definition 1
The *octant subdivision level* (OSL) is defined as the number of decompositions from the initial grid system. For instance, OSL of every octant in the initial grid system is assigned as zero and levels of all direct children octants are assigned as one.

In this study, it is assumed that element size conditions are provided in terms of $(\mathbf{P}_i,\ h_i)$, where $\mathbf{P}_i$ and h_i are the position to be refined and the element size at that position, respectively. Then, such element size conditions are changed into the refinement level conditions in terms of $(\mathbf{P}_i, L_i)$, where L_i is an integer value of division level of octant size according to the element size value h_i. Recursive decomposition is carried out after all refinement conditions are specified.

3.2. Conversion of octant to hexahedral element

After an initial octree structure is constructed as described in the previous section, conversion of octants into hexahedral elements is carried out through the following three steps, namely, (i) a simple conversion process, (ii) detection and classification of transition elements, and (iii) substitution of transition elements with appropriate templates.

First, in the simple conversion process of step (i), each octant with no children octants is simply converted into a hexahedral element. In the case that children octants exist, which means that the region of the octant is occupied by higher-order octants, each child octant is converted into a hexahedral element. The second step, the detection and classification of transition elements play a crucial role in the automatic refinement process. As can be seen in Figure 12, the recursive decomposition process creates irregular nodes at the interface between the subdivided and surrounding regions, which violate the conformity condition. Thus, the existence and location of such irregular nodes must be properly detected. For this purpose, the terms *element subdivision level* (ESL), *node subdivision level* (NSL), and *refinement control node* (RCN) are defined as follows:

Definition 2
The ESL is defined as the subdivision level of the octant which has been converted into a hexahedral element.

Definition 3
The NSL is defined as the maximum ESL among the attached elements to a corresponding node.

Definition 4
In an element, it might occur in which the NSL of nodes is different from each other. In this case, a node whose NSL is greater than that of other elemental nodes is defined as the RCN.

Figure 14 illustrates the determination of both subdivision levels and the detection of RCNs. As shown, once RCNs have been determined, elements that surround the RCNs are labelled

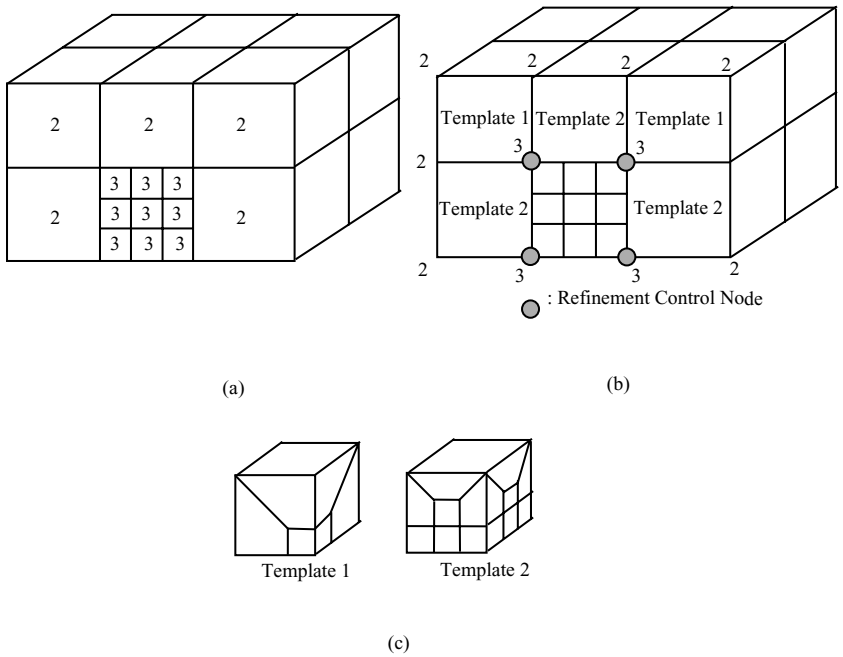

Figure 14. Schematic diagrams of the determination of: (a) the ESL; (b) the NSL; and (c) the templates required for satisfying comformity conditions.

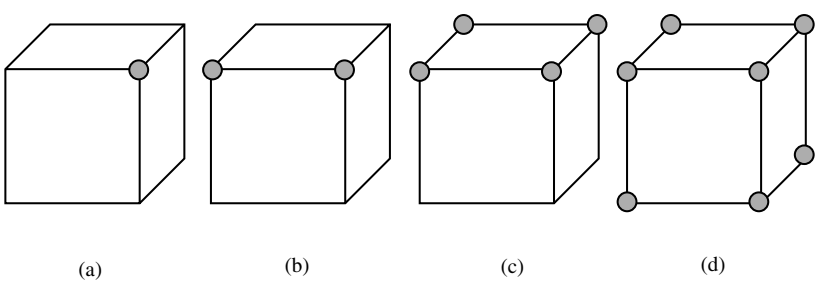

Figure 15. Schematic diagrams of the four major RCN configurations in three-dimensions: (a) vertex; (b) edge; (c) face; and (d) solid modes.

as transition elements. Then, such transition elements are classified into appropriate transition modes depending on the RCN configuration and appropriate templates are applied. This process can be simply extended to the three-dimensional case, but a much greater number of RCN configurations can exist in three-dimensions. Therefore, as an initial attempt, only four major RCN configuration modes proposed by Schneider *et al.* [32] were used in the present investigation. Figure 15 shows the four major RCN configurations, each named as vertex, edge, face, and solid mode, respectively.

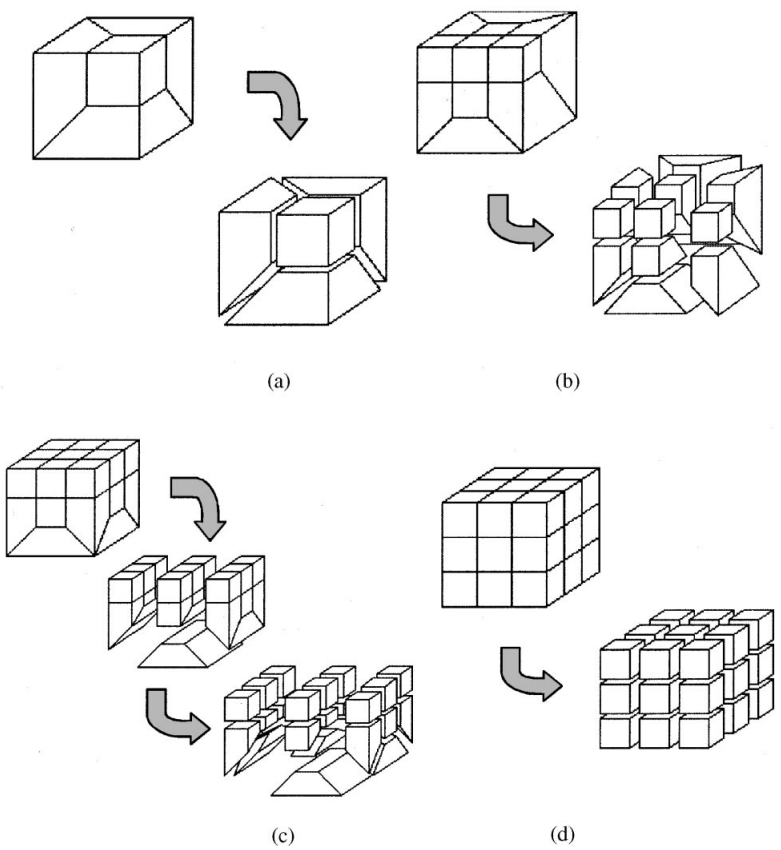

Figure 16. Schematic diagrams describing the decomposition scheme of each template for the corresponding configuration mode: (a) vertex; (b) edge; (c) face; and (d) solid modes.

Figure 16 shows the decomposition scheme of each template for the corresponding configuration mode. It should be noted that RCN configurations not consistent with one of the four major modes, will be transformed into consistent ones as shown in Figure 17. By doing this, the robustness of refinement can be ensured, but propagation of the refinement region into unrefined regions is unavoidable. Thus, the development of templates corresponding to all RCN configuration modes is required in the future.

3.3. Mesh generation example

In order to examine the applicability and stability of the refinement algorithm used in this study, the refinement process was carried out for a cubical model under three different refinement conditions. Figure 18 shows the three different refinement conditions and resultant locally refined hexahedral mesh systems. Figure 19 shows an example of locally refined hexahedral mesh generation for a more practical case. This is the same example as in Figure 10 except that a locally refined core mesh system is initially used. From these results, it was found that

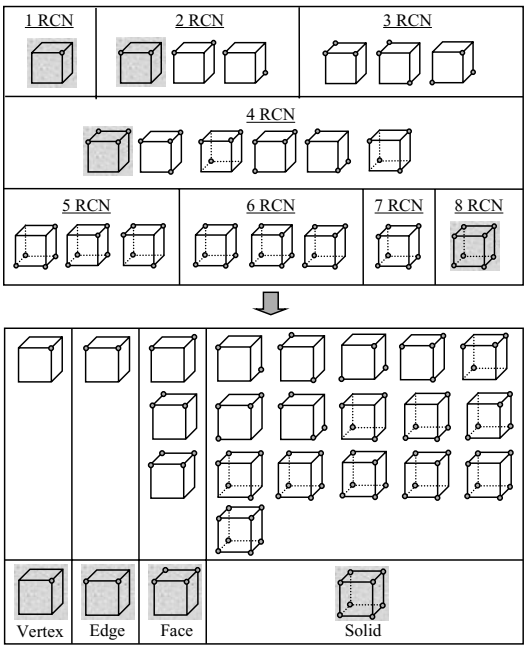

Figure 17. Schematic description of the transformation process from inconsistent RCN configurations to one of the four major modes.

the mesh refinement process can be successfully applied to the generation of locally refined hexahedral mesh systems with general geometries.

4. METAL FORMING SIMULATION EXAMPLES

As mentioned, the developed hexahedral mesh generator was implemented into CAMP*form-3D*, which is a three-dimensional metal forming simulator. In this study, several three-dimensional metal forming analyses were carried out using CAMP*form-3D* [43] to check the applicability of the developed hexahedral mesh generator. Also, in order to investigate the effectiveness of locally refined mesh generation, a comparative study of indentation analyses was carried out.

4.1. Examples: uniformly sized hexahedral remeshing

Figure 20 shows the analysis conditions used for the three-dimensional benchmark simulation. As can be seen, this simulation was carried out through two steps, namely, preform upsetting and backward extrusion. It was assumed that the die velocity and friction factor were 1.0 mm/s and 0.25. The hardening factor and exponent of flow equation were assumed to be 763.1 N/mm^2 and 0.245, respectively. It can be expected that large deformation will occur during the second backward extrusion process. In fact, the completion of simulation was

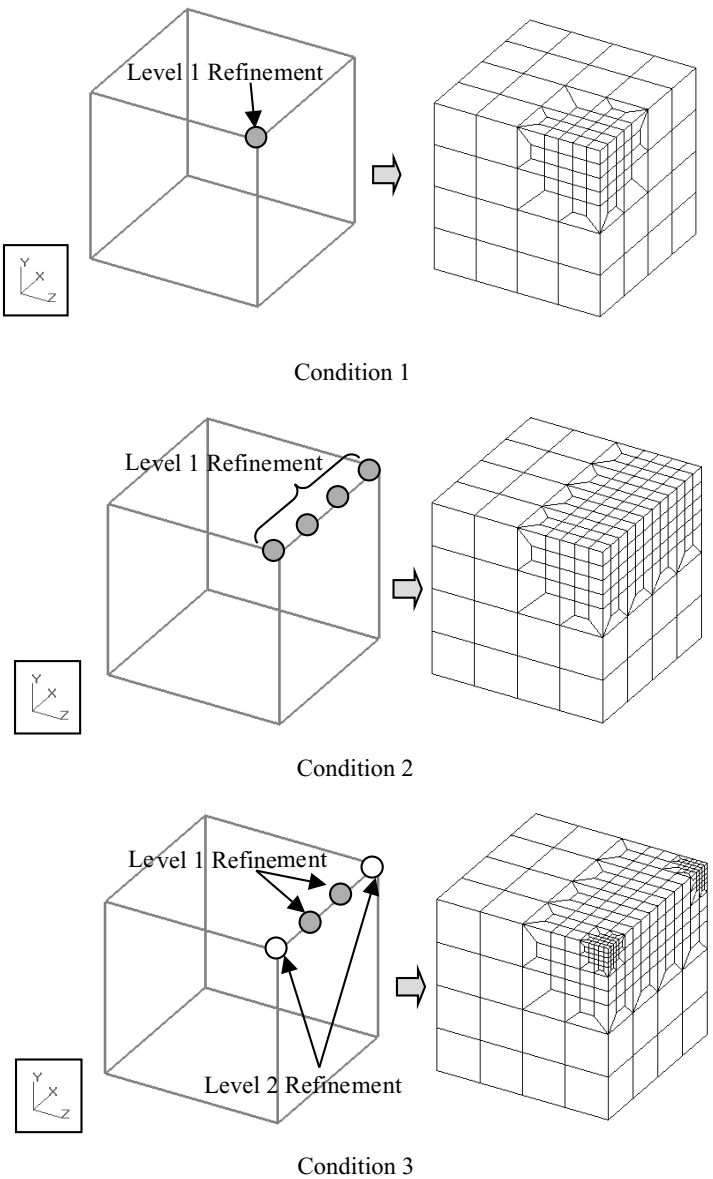

Figure 18. Different refinement conditions and resultant locally refined hexahedral mesh systems.

achieved with five remeshing stages as shown in Figure 21. The maximum effective strain at the final stage was calculated to be 2.83.

Figure 22 gives the analysis conditions for the closed-die spur gear forging simulation. As shown in this figure, it was assumed that the material was Al6061-T4 aluminium alloy and

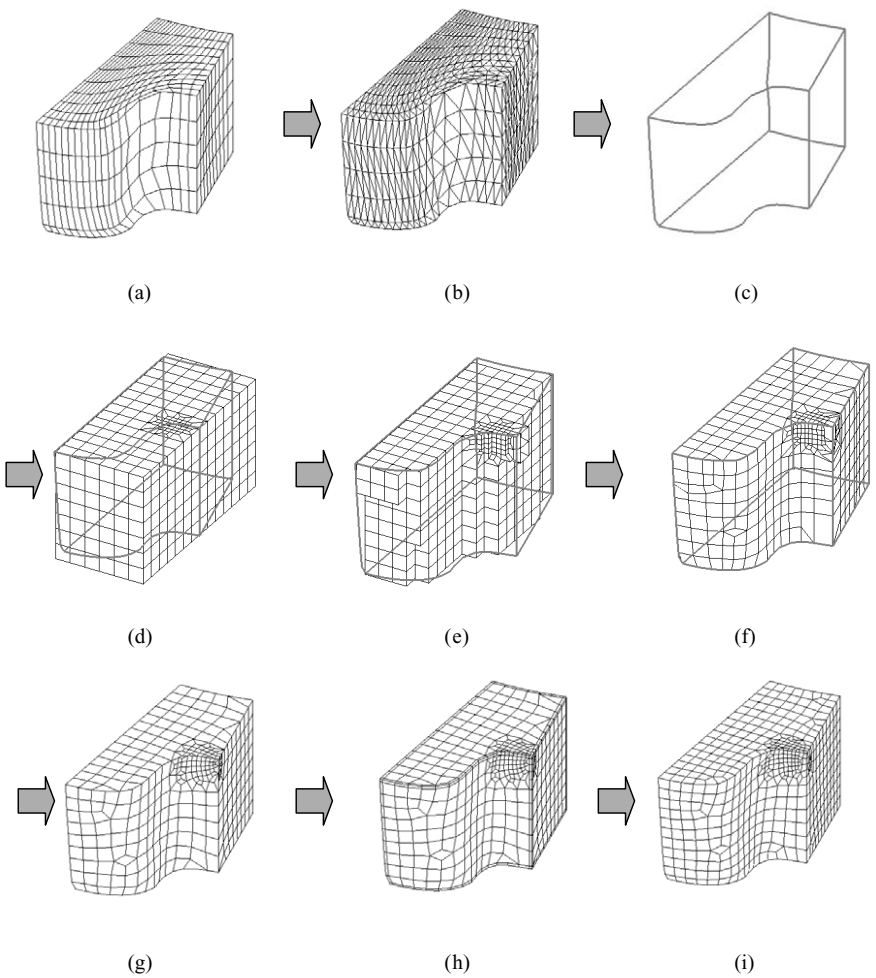

Figure 19. The procedure of locally refined hexahedral mesh generation for remeshing at an intermediate stage of spur gear forging simulation: (a) old mesh; (b) triangular boundary mesh; (c) CV/CL; (d) initial core mesh; (e) core mesh after removal of exterior elements; (f) boundary fitted mesh; (g) boundary fitted mesh after smoothing; (h) SEL generated mesh; and (i) final mesh.

the die velocity and friction factor were 1.0 mm/s and 0.2, respectively. This simulation was successfully completed with only one remeshing process and complete filling was achieved as shown in Figure 23. The maximum effective strain at the final stage was calculated to be 2.63.

The third simulation example is that of closed-die connecting rod forging. This simulation was carried out through the two steps shown in Figure 24. As shown in this figure, this analysis was carried out with the same material and die velocity condition as in the case of spur gear example but the friction factor was assumed to be 0.16. In this case, seven

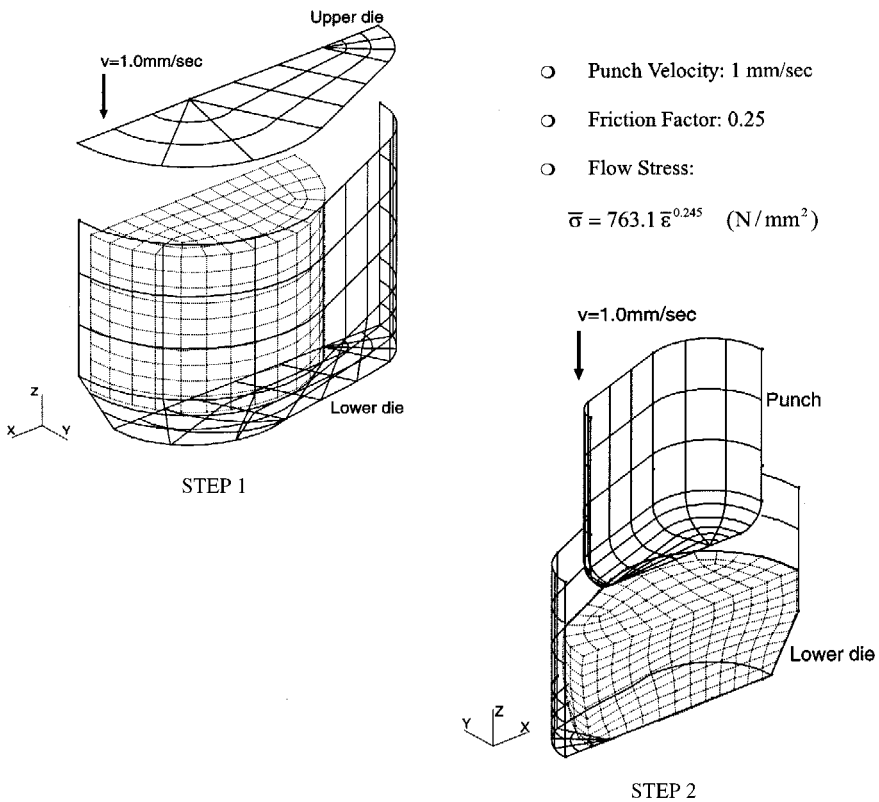

Figure 20. Analysis conditions of the three-dimensional benchmark simulation.

remeshing stages were required for the completion of simulation and the maximum effective strain at the final stage was calculated to be 4.61. Figure 25 shows the final deformed shape.

From these three results, it can be seen that the developed hexahedral mesh generator can be successfully used for remeshing in three-dimensional simulation of practical metal forming processes.

4.2. Examples: locally refined hexahedral remeshing

In this study, indentation analyses with a spherical punch as shown in Figure 26 were carried out for the purpose of investigating the effectiveness of locally refined mesh systems compared to uniformly sized mesh systems during the remeshing process. For this, the analysis using an initial mesh system with 512 elements was carried out until remeshing was required and then it was continued by remeshing to different mesh systems. Figure 27 shows four uniformly sized mesh systems with 574, 1088, 2179, and 4056 elements and two locally refined mesh systems with 1023 and 1099 elements obtained by remeshing. Refinements of Case 5 and Case 6 were based on Z^2 *posteriori* error analysis results and the distribution of effective strain rate gradient, respectively.

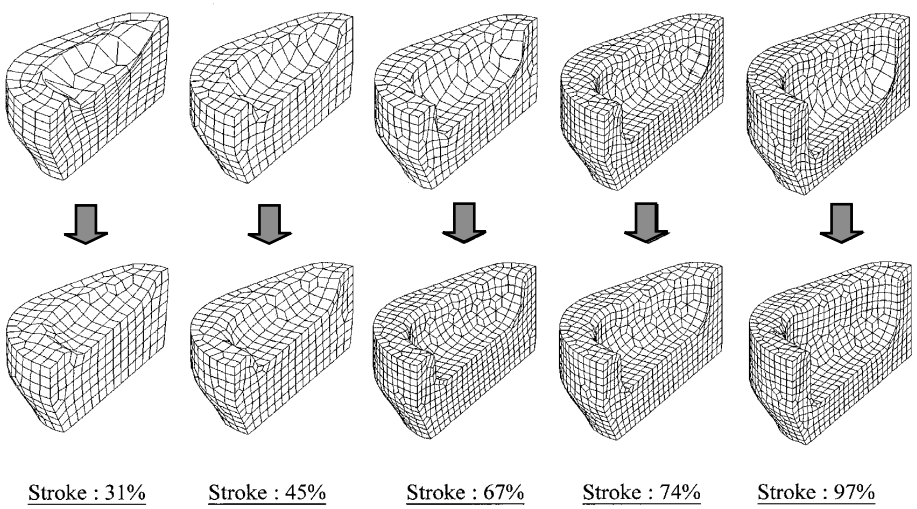

Figure 21. Configurations of the original and reconstructed mesh systems during the second backward extrusion process of the benchmark simulation.

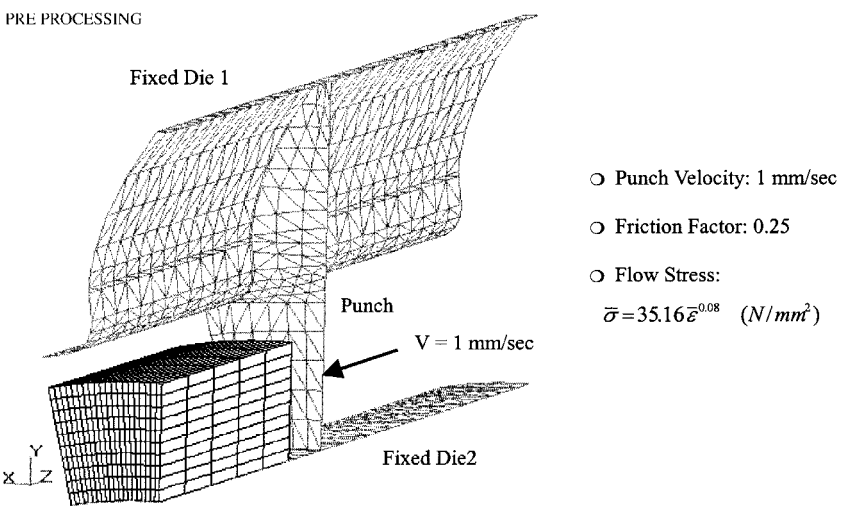

Figure 22. Analysis conditions of the closed-die spur gear forging simulation.

In particular, in the current investigation, total error energy, global relative error energy, forming load, and CPU time were examined for each as summarized in Table I. Here the total error energy and global relative energy are represented as percentages with respect to those values calculated for the initial mesh system with 512 elements immediately before remeshing. Total error energy, $\|e\|$, and global relative error energy η are defined

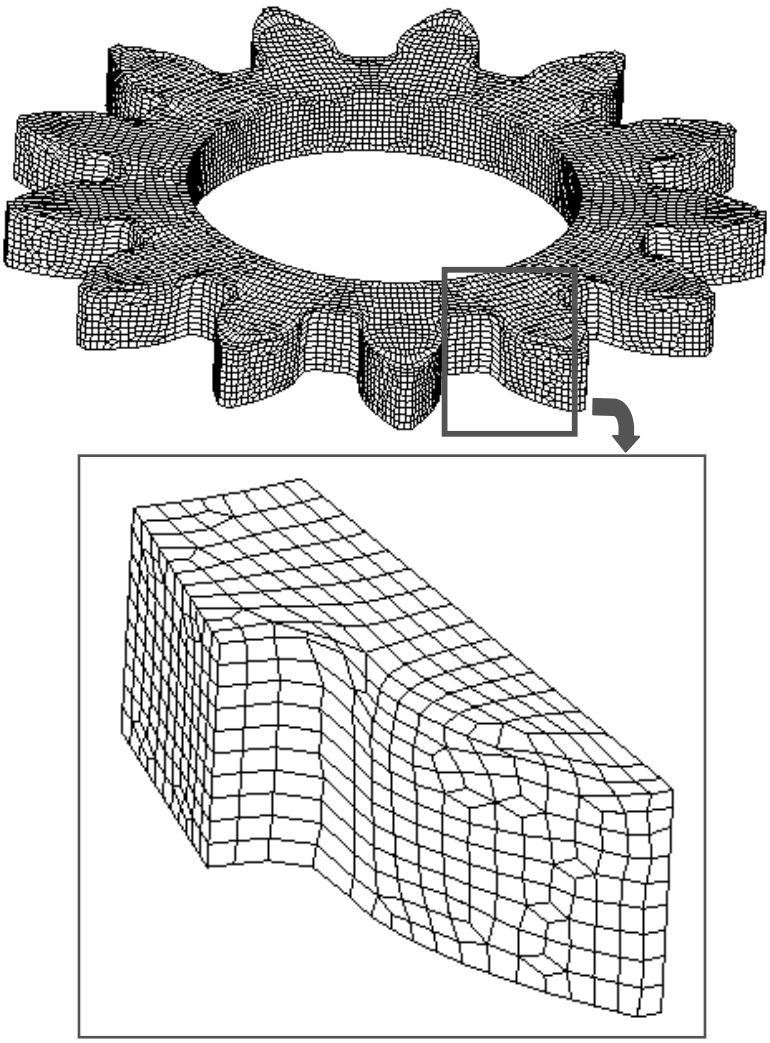

Figure 23. Deformed shape at the final stage of the closed-die spur gear forging simulation.

as follows:

$$\|e\| = \left[\int_{\Omega} \frac{2\bar{\sigma}}{3\dot{\bar{\varepsilon}}} (\dot{\varepsilon}^* - \hat{\dot{\varepsilon}})^{\mathrm{T}} (\dot{\varepsilon}^* - \hat{\dot{\varepsilon}}) \, \mathrm{d}\Omega \right]^{1/2}, \quad \eta = \frac{\|e\|}{\|U\|} \tag{4}$$

Here, $\dot{\varepsilon}^*$, $\hat{\dot{\varepsilon}}$, and $\|U\|$ are the recovered solution, the approximate FEM solution, and the total strain energy, respectively.

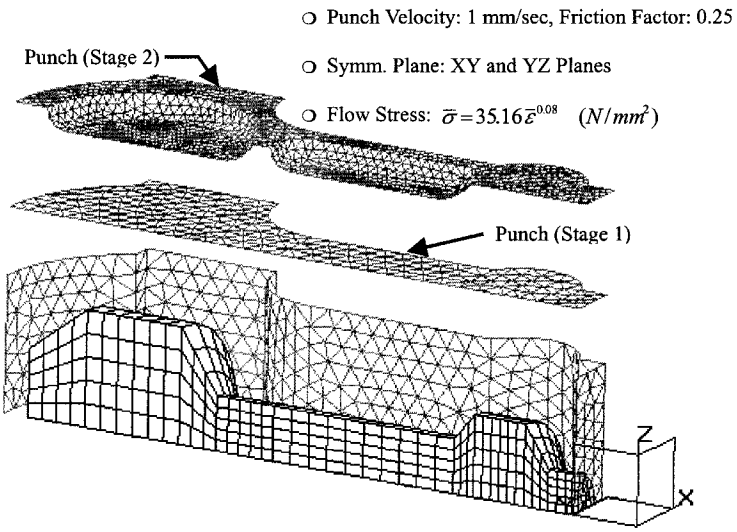

Figure 24. Analysis conditions of closed-die connecting rod forging simulation.

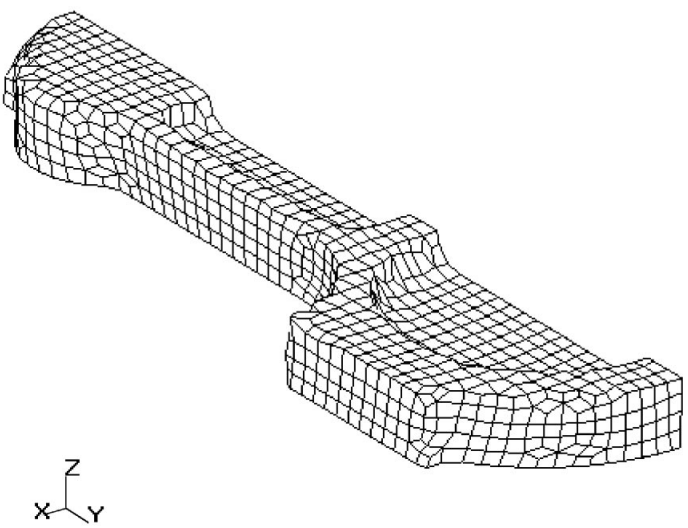

Figure 25. Deformed shape at the final stage of the closed-die connecting rod forging simulation.

As can be seen in Table I, for uniformly sized mesh systems, the percentages of total error energy and global relative error energy decrease and the loads increase with increasing number of elements. For refined mesh systems, the percentages of both error energies are less than that for the uniformly sized mesh system with 1088 elements and the loads are much closer to that of the mesh system with 4056 elements compared to those for the cases with

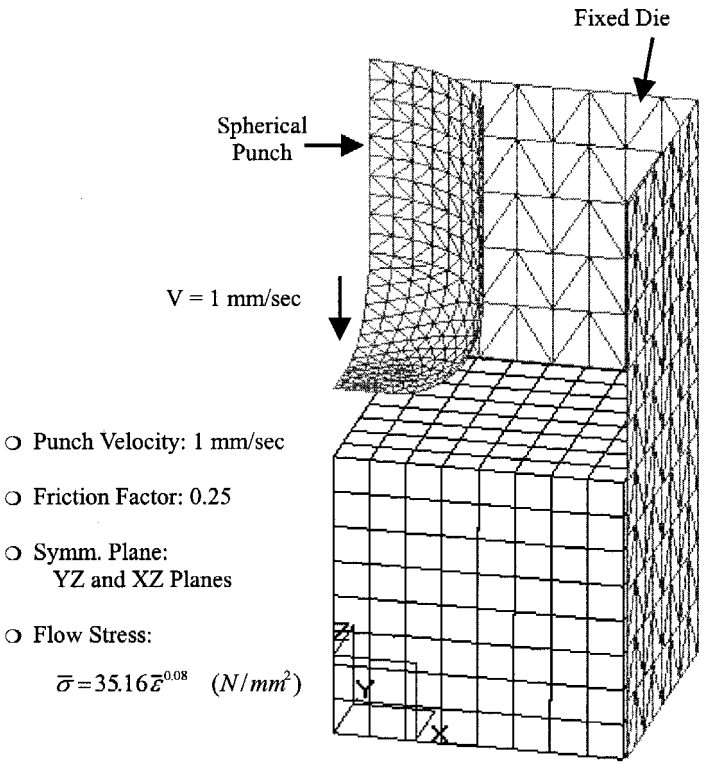

Figure 26. Analysis conditions of indentation simulation.

574, 1088 and 2179 elements. This shows that locally refined mesh systems are more efficient in terms of computational effort compared to uniformly sized mesh systems.

5. CONCLUSIONS

In the present investigation, a hexahedral mesh generator based on the master grid approach and octree-based refinement scheme was developed for remeshing in three-dimensional metal forming simulations. Several metal forming analyses were carried out using the developed hexahedral mesh generators and from this, the following conclusions can be made:

1. By integrating the master grid approach and octree-based refinement scheme, both uniformly sized and locally refined hexahedral mesh systems can be successfully generated using the developed hexahedral mesh generator.
2. From the benchmark, closed-die spur gear, and connecting rod forging analyses, it was found that the developed hexahedral mesh generator can be successfully used for remeshing in three-dimensional analyses of practical metal forming processes.

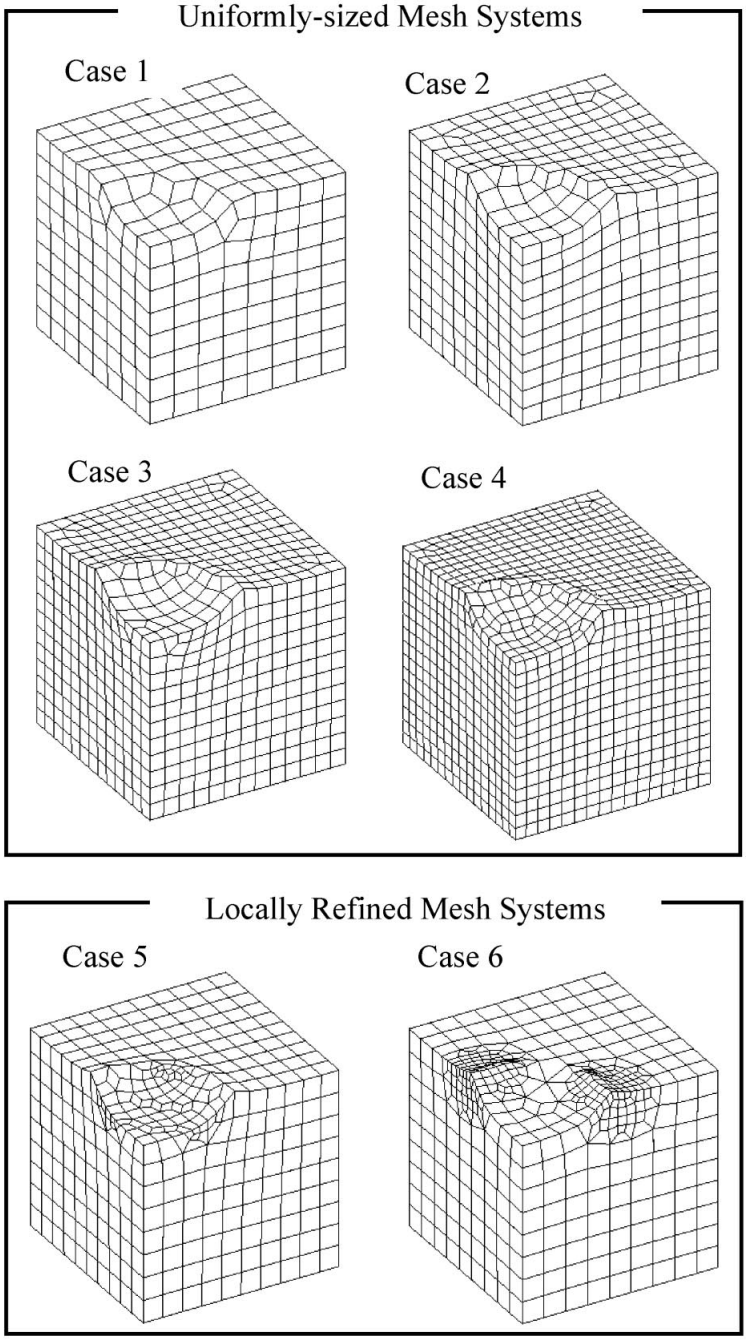

Figure 27. Uniformly sized and locally refined mesh systems in indentation analyses.

Table I. Summary of indentation analysis results.

	Uniformly sized mesh			Refined mesh		
Mesh system	Case 1	Case 2	Case 3	Case 4	Case 5	Case 6
No. of elements	574	1088	2179	4056	1023	1099
Total error energy (%)	94	79	64	52	74	75
Global relative error energy (%)	70	59	48	39	54	55
Load at 18.3 mm stroke	1432	1438	1503	1550	1545	1524
CPU time(CrayT3E;s)	678	2563	11739	41999	2667	2890

3. For the case of indentation analysis examined, it was found that locally refined mesh system was more efficient while maintaining the accuracy of forming load compared to uniformly sized mesh system.

ACKNOWLEDGEMENT

The authors wish to acknowledge the support from the BK (Brain Korea) 21 project.

REFERENCES

1. Buell WR, Bush BA. Mesh Generation—a survey. *Transactions of the* ASME, *Journal of Engineering for Industry* 1973; **95**:332–338.
2. Thacker WC. A brief review of techniques for generating irregular computational grids. *International Journal for Numerical Methods in Engineering* 1980; **15**:1335–1341.
3. Ho-Le K. Finite element mesh generation methods: a review and classification. *Computer-Aided Design* 1988; **20**:27–38.
4. Shephard MS. Approaches to the automatic generation and control of finite element meshes. *Applied Mechanics Reviews* 1988; **40**:169–185.
5. George PL. *Automatic Mesh Generation: Application to Finite Element Methods*. Wiley: New York, 1991.
6. Cavendish JC, Field DA, Frey WH. An approach to automatic three-dimensional finite element mesh generation. *International Journal for Numerical Methods in Engineering* 1985; **21**:329–347.
7. Baker TJ. Automatic mesh generation for complex three-dimensional regions using a constrained regions using a constrained Delaunay triangulations. *Engineering Computations* 1989; **5**:161–175.
8. Wright JP, Jack AG. Aspects of three-dimensional constrained Delaunay meshing. *International Journal for Numerical Methods in Engineering* 1994; **37**:1841–1861.
9. Conti P, Tomizawa M, Yoshii A. Generation of oriented three-dimensional Delaunay grids suitable for the control volume integration method. *International Journal for Numerical Methods in Engineering* 1994; **37**:3211–3227.
10. Golias NA, Tsiboukis TD. An approach to refining three-dimensional tetrahedral meshes based on Delaunay transformations. *International Journal for Numerical Methods in Engineering* 1994; **37**:793–812.
11. Yerry MA, Shephard MS. Automatic three-dimensional mesh generation by the modified octree technique. *International Journal for Numerical Methods in Engineering* 1984; **20**:1965–1990.
12. Shephard MS. Automatic and adaptive mesh generation. *IEEE Transactions on Magnetics* 1985; **21**: 2482–2489.
13. Shephard MS, Georges MK. Automatic three-dimensional mesh generation by the finite octree technique. *International Journal for Numerical Methods in Engineering* 1991; **32**:709–749.
14. Jung YH, Lee K. Tetrahedron-based octree encoding for automatic mesh generation. *Computer-Aided Design* 1993; **25**:141–153.
15. Joe B. Tetrahedral mesh generation in polyhedral regions based on convex polyhedron decompositions. *International Journal for Numerical Methods in Engineering* 1994; **37**:693–713.
16. Moller P. On advancing front mesh generation in three dimensions. *International Journal for Numerical Methods in Engineering* 1985; **38**:3519–3551.
17. Chae SW, Bathe KJ. On automatic mesh refinement in finite element analysis. *Computers and Structures* 1989; **32**:911–936.

18. Jin H, Tanner RI. Generation of unstructured tetrahedral meshes by advancing front technique. *International Journal for Numerical Methods in Engineering* 1993; **36**:1805–1823.
19. David RW. Automated hexahedral mesh generation by virtual decomposition. *Proceedings of the 4th International Meshing Roundtable*, 1995; 165–176.
20. Blacker T. The Cooper tool. *Proceedings of the 5th International Meshing Roundtable*, 1996; 13–29.
21. Lai M, Steven EB, Sjaardema G, Tautges T. A multiple source and target sweeping method for generating all hexahedral finite element meshes. *Proceedings of the 5th International Meshing Roundtable*, 1996; 217–228.
22. Chiba N, Nishigaki I, Yamashita Y, Takizawa C, Fujishiro K. An automatic hexahedral mesh generation system based on the shape-recognition and boundary-fit methods. *Proceedings of the 5th International Meshing Roundtable*, 1996; 281–290.
23. Liu SS, Rajit G. Basic logical bulk shapes (BLOBs) for finite element hexahedral mesh generation. *Proceedings of the 5th International Meshing Roundtable*, 1996; 291–306.
24. Mitchell SA. High Fidelity interval assignment. *Proceedings of the 6th International Meshing Roundtable*, 1997; 33–44.
25. Blacker TD, Meyers RJ, Sams and wdges in pastering: a 3D hexahedral mesh generation algorithm. *Engineering with Computers* 1993; **2**:83–93.
26. Leland RW, Darryl JM, Ray WM, Mitchell SA, Timothy JT. The geode algorithm: combining hex/tet plastering, dicing and transition elements for automatic, all-hex mesh generation. *Proceedings of the 7th International Meshing Roundtable*, 1998; 515–521.
27. Meyers RJ, Timothy JT, Tuchinsky PM. The Hex-Tet hex-dominant meshing algorithm as implemented in CUBIT. *Proceedings of the 7th International Meshing Roundtable*, 1998; 151–158.
28. Timothy JT, Mitchell SA. Whisker weaving: invalid connectivity resolution and primal construction algorithm. *Proceedings of the 4th International Meshing Roundtable*, 1995; 115–127.
29. Murdoch P, Steven EB. The spatial twist continuum. *Proceedings of the 4th International Meshing Roundtable*, 1995; 243–251.
30. Tautges TJ, Blacker T, Mitchell SA. The whisker weaving algorithm: a connectivity-based method for constructing all-hexahedral finite element meshes. *International Journal for Numerical Methods in Engineering* 1996; **39**:3327–3349.
31. Folwell NT, Mitchell SA. Reliable whisker weaving via curve contraction. *Proceedings of the 7th International Meshing Roundtable*, 1998; 365–378.
32. Schneiders R, An algorithm for the generation of hexahedral element meshes based on an octree technique. *Proceedings of the 6th International Meshing Roundtable*, 1997; 183–194.
33. Lee YK, Yang DY. Development of a grid-based mesh generation techniques and its application to remeshing during the finite element simulation of a metal forming process. *Engineering Computations* 1999; **16**:316–336.
34. Zienkiewicz OC, Taylor RL. *The Finite Element Method: Basic Formulation and Linear Problems*. McGraw-Hill: New York, 1989.
35. Zienkiewicz OC, Zhu JZ. A simple error estimator and adaptive procedure for practical engineering analysis. *International Journal for Numerical Methods in Engineering* 1987; **24**:337–357.
36. Zienkiewicz OC, Zhu JZ. Adaptivity and mesh generation. *International Journal for Numerical Methods in Engineering* 1991; **32**:783–810.
37. Georges MK, Shephard MS. Automated adaptive two-dimensional system for the hp-version of the finite element method. *International Journal for Numerical Methods in Engineering* 1991; **32**:867–893.
38. Remondini L, Trompette P, Leon JC, Noel F. A new concept in two-dimensional auto-adaptive mesh generation. *International Journal for Numerical Methods in Engineering* 1994; **37**:2841–2855.
39. Connell SD, Holmes DG. Three-dimensional unstructured adaptive multigrid scheme for the Euler equations. *AIAA Journal* 1994; **32**:1626–1632.
40. Lee CK, Lo SH. An automatic adaptive refinement procedure using triangular and quadrilateral meshes. *Engineering Fracture Mechanics* 1995; **50**:671–686.
41. Sandhu JS, Liebowitz H. Mesh adaptation using a four-noded quadrilateral plate bending element. *Engineering Fracture Mechanics* 1995; **50**:737–758.
42. Yang DY, Yoon JH, Lee NK. Modular remeshing: a practical method of 3-D remeshing in forging of complicated parts. *Advanced Techniques in Plasticity* 1990:171–178.
43. Kwak DY, Kim SY, Im YT, Chae SW. Development of three-dimensional analysis system for various metal forming processes. *KSTP Transactions of Materials Processing* 2000; **9**:761–768.
44. Kim SY, Im YT. Three-dimensional finite element simulation of shape rolling of bars. *International Journal of Forming Processes* 2000; **3**:253–278.
45. Kobayashi S, Oh SI, Altan T. *Metal Forming and the Finite Element Method*. Oxford University Press: New York, 1989.

